RSC Advances

PAPER

View Article Online
View Journal | View Issue

Cite this: *RSC Adv.*, 2017, **7**, 23671

Preparation of *in situ* forming and injectable alginate/mesoporous Sr-containing calcium silicate composite cement for bone repair

Manle Qiu, †[a] Daoyun Chen,†[a] Chaoyong Shen,†[b] Ji Shen,[a] Huakun Zhao[a] and Yaohua He*[a]

Injectable biomaterials to aid bone regeneration are worth investigating in bone tissue engineering due to minimized invasive damages. In this study, a novel *in situ* formed composite cement consisting of alginate and Sr-containing mesoporous calcium silicate nanoparticles (mSCS) has been designed. Firstly, mSCS were fabricated with Sr-substitution for Ca in mesoporous calcium silicate nanoparticles. The morphology, particle size, element mapping and mesoporous structure of the mSCS nanoparticles were characterized. The results showed that the nanoparticles were in the range from 200 nm to 300 nm, and had a surface area of about 312 m^2 g^{-1}. Then the mSCS materials were mixed with a sodium alginate solution. The alginate component in the composite cement was internally crosslinked by locally released Ca^{2+}/Sr^{2+} cations from mSCS through the addition of D-gluconic acid δ-lactone (GDL). Characterization results showed that GDL accelerated the gelation rate of cement and thus increased the injectability coefficient to more than 90% after 2 minutes of setting. The higher amount of GDL enhanced the tridimensional network formation rate and improved the compressive strength and Young's modulus of the cement. In addition, scanning electron microscopy (SEM) observations demonstrated that the alginate hydrogel provided extra micropores (tens of micrometers) for cell growth. The mSCS induced fast bone-like apatite deposition on the surface of all the cements after 3 days of SBF immersion. *In vitro* human bone mesenchymal stem cell (hBMSC) tests, including Cell Counting Kit-8 (CCK-8) assay and alkaline phosphatase (ALP) activity evaluation, revealed that the injectable mSCS–alginate cement had significant biocompatibility and low cytotoxicity, and moreover could support hBMSC proliferation and osteogenesis differentiation.

Received 30th December 2016
Accepted 23rd March 2017

DOI: 10.1039/c6ra28860j

rsc.li/rsc-advances

Introduction

Tissue engineering techniques with the aid of biomaterials provide an alternative and promising strategy to regenerate bones.[1,2] Biomaterials, including naturally occurring materials and synthetic materials, are basically fabricated into preformed porous scaffolds or injectable systems to fit in bone defects.[3,4] It is acknowledged that injectable systems can achieve a minimized invasive damage from open surgery, and improve the patient's comfort compared to preformed scaffolds. Moreover, directly injected biomaterials can fit irregular defects in a better manner, while scaffolds need shaping to match, and thus cause a longer surgery time and a higher risk of surgery-related injuries.[5–7] However, injectable biomaterials, including cements or hydrogels, have their own drawbacks that limit their osteogenesis properties. For instance, solidified cements generate heat from the hydration reaction that may impair the surrounding tissues, and the cements lack a macroporous structure for cell penetration and growth.[8] In contrast, injectable hydrogels are able to support cellular activities in a water-rich microenvironment. But hydrogels, nevertheless, are too weak to bear a load and are seldom used for hard bone regeneration.[9] Compounding ceramic particles into a hydrogel matrix was reported to enhance their mechanical strength and bioactivity when the fragile water-filled structure is maintained.[10–12]

Mesoporous calcium silicate (mCS) possesses fascinating texture properties, like high surface areas and adjustable nanopores, and hence mCS exhibits an improved bioactive response compared to conventional CS materials. In addition, the skeletal applications of mCS have been confirmed in a battery of literature because of its enhanced apatite-mineralization ability, drug delivery property and osteo-stimulation.[13–16] In order to increase the chemical stability of mCS, other elements were incorporated to slow down the ion dissolution and degradation rate. These additional elements, such

[a]*Department of Sports Medicine, Shanghai Jiao Tong University Affiliated Sixth People's Hospital, Shanghai 200233, China. E-mail: heyaohuadoctor@163.com; Fax: +86 021 64701361; Tel: +86 021 64369181*

[b]*Department of Gastrointestinal Surgery, West China Hospital, Sichuan University, Chengdu 610041, China*

† All authors contributed equally to this work.

as zinc, strontium, magnesium, cerium and so on,[17–19] have indicated certain physiochemical and biological functions. Thereinto, Sr is an important trace element in the human body and plays a big part in bone remodeling. Sr-based drugs are clinically applied to promote osteoblast replications while inhibiting bone resorption by osteoclasts.[20,21] Therefore, Sr has been substituted for the Ca species in Ca-based bioceramics and bioglasses to achieve better osteogenesis performances.[22] For example, Gentleman *et al.* reported results of Sr-incorporated bioactive glasses (BG) from which they may have an anabolic effect on osteoblasts and an anti-catabolic effect on osteoclasts, which is similar to the anti-osteoporosis drug strontium ranelate.[23] Zhu *et al.* prepared mesoporous Sr–$CaSiO_3$ powder materials with different Sr substitution amounts. They found that Sr stabilized the pH microenvironment and a higher Sr content stimulated the ALP activity of MC3T3-E1 cells.[18]

Alginate is one interesting type of natural polymer applied in soft tissue engineering and bio-molecular delivery.[24] To form hydrogels, alginate is preferred because of its easy gelation through cation-crosslinking.[25] Ca^{2+} ions are biosafe in most circumstances and thus became the most common cation crosslink agent due to the simplicity and low-cost as well. Other divalent cations, such as Ba^{2+}, Sr^{2+} and Cu^{2+}, *etc.*, can also serve as linkers.[26–28] These divalent cations react with carboxylic groups on alginate biopolymer chains to form a tridimensional stable network. According to previous studies, Sr^{2+} had a higher gelation efficiency by comparison with Ca^{2+}. The use of strontium resulted in an increased stability and strength of a high percentage of guluronic acid residues (high-G) alginate.

On the other hand, a relatively larger volume of homogeneous alginate hydrogel can be fabricated only if the cations were released in a controlled way instead of by direct crosslinker ion injection (*i.e.* $CaCl_2$). The method of dropping the alginate solution into a $CaCl_2$ solution to form an alginate gel has been extensively used though; this "external gelation" (or heterogeneous gelation by an external Ca(II) source) was found to lead to heterogeneous gel structures with a more rigid surface layer than the center layer due to the hindrance of Ca species diffusion through the surface layer. In contrast, the alginate hydrogel obtained by the "internal gelation" method suggested a much higher stability and homogeneity.[29,30] The "internal gelation" method is usually referred to as the progressive release of acid internally, which, in turn, reacts with the calcium salt to release Ca(II) ions. For instance, D-gluconic acid δ-lactone (GDL) is one common agent that produces weak acids, through hydrolysis, that can react with calcium salts, like $CaCO_3$, $CaSO_4$ and hydroxyapatite.[31,32] Han Yan *et al.* have prepared injectable and *in situ* forming composite calcium silicate/sodium alginate hydrogels using GDL.[33] The gelling time, compressive properties and swelling behaviors of the composite hydrogel system could be controlled and regulated by varying the contents of CS and GDL.

In this study, Sr-incorporated mCS nanoparticles were synthesized and then added into an alginate matrix to form an injectable composite cement. It is reasonable to assume that Ca^{2+} and Sr^{2+} can be internally released from the mSCS network *via* GDL hydrolysis, and therefore homogeneously crosslink sodium alginate molecules. The gelled alginate is expected to enhance the injectability and stability of the mSCS–alginate composite cement. More importantly, mSCS–alginate hydrogel composites with an integral unity after injection strongly maintain their shapes and structures.

Experimental methods

Preparation of mesoporous Sr-containing calcium silicate nanoparticles (mSCS)

The synthesis of Sr-doped mesoporous calcium silicate (mSCS) nanoparticles followed the published protocol with modifications.[34] Briefly, 6.6 g cetyltrimethylammonium bromide (CTAB) and 12 mL NH_3H_2O were dissolved in 600 mL ddH_2O with stirring for 30 min. Then, 30 mL of tetraethyl orthosilicate (TEOS), 25 g of $Ca(NO_3)_2 \cdot 4H_2O$ and 7.16 g of $SrCl_2 \cdot 4H_2O$ were added with vigorous stirring for 3 h. The products were collected by filtration and washed three times each with ddH_2O and ethanol. Then, the collected powders were dried at 60 °C overnight and calcined at 550 °C for 5 h.

Characterizations of mSCS materials

Transmission electron microscopy (TEM) was performed with a JEM-2010 electron microscope operated at an acceleration voltage of 200 kV. Elemental mapping of the TEM images and energy dispersive spectrometry (EDS) analysis were carried out to evaluate the compositions in mSCS nanoparticles. N_2 adsorption–desorption isotherms were obtained on a Micromeritics Tristar 3020 at 196 °C under continuous adsorption conditions. Brunauer–Emmett–Teller (BET) and Barrett–Joyner–Halenda (BJH) methods were used to determine the surface area and pore size distribution.

Fabrication of mSCS/alginate composite cement

Alginate sodium powder was dissolved in ddH_2O to form a 5 w/v% solution. Then 0 g, 0.05 g, and 0.1 g of GDL were added to 2 g of the alginate solution respectively and control the release rate of Ca^{2+}/Sr^{2+} from mSCS. According to a previous viscosity estimation and investigation, 0.4 g of synthesized mSCS nanoparticle powders were then mixed into the above solutions. Homogeneously stirred pastes were designated as mSCS-A-0, mSCS-A-0.05 and mSCS-A-0.1, respectively.

Injectability, shrinkage and compressive strength

Newly formed pastes were settled for gelation first. After 10 s or 120 s the pastes were transferred to a commercial 10 mL syringe gelation and extruded (100 N, 10 mm min^{-1}, CMT6104). The injectability coefficient (I) was defined as:

$$I = [(M_0 - M)/M_0] \times 100 \quad (1)$$

where M_0 is the initial mass of the paste loaded and M is the mass remaining in the syringe after extrusion. Triplicates for each sample were tested and the results were expressed as a mean ± standard deviation (SD).

Cylindrical specimens of the composite cement were made in molds 10 mm in height and 15 mm in diameter. The compressive strength of the specimens after gelling for 2 h was determined by an Electronic Universal Testing Machine (Zwick), for which the compressive speed was set at 0.5 mm min^{-1} and no preload was applied. Five replicates were averaged for each sample.

The height and diameter of vacuum-dried cement samples were then measured to calculate the sample shrinkage (S) as the following formulation describes:

$$S = [(H_0 - H) + (R_0 - R)]/2 \quad (2)$$

where H_0 and R_0 are the pristine height/diameter of wet cement, and H and R are the height/diameter of dried cement.

Compressive strengths of the dried samples were tested in the same way as with the wet cement.

In vitro apatite deposition

Simulated body fluid (SBF) containing ion concentrations similar to those in human blood plasma were prepared according to previous protocol.[35] The mSCS-A-0, mSCS-A-0.05 and mSCS-A-0.1 cements were soaked in SBF (V_{SBF}/W_{sample} = 200 mL g^{-1}) at 37 °C for 3 days. The SBF solution was not replenished throughout the soaking period. After immersing, cement samples were rinsed with ddH_2O and dried. SEM and EDS were used to observe the surface morphology and compositions.

In vitro cell viability

Primary human bone marrow-derived mesenchymal stem cells (hBMSCs) were isolated as previously described.[36] All the experiments were performed in compliance with the Experimental Safety Guidelines of Shanghai Jiao Tong University School of Medicine. The use of human samples was approved by the ethical committee of the Sixth People's Hospital, Shanghai Jiao Tong University School of Medicine.

To investigate the proliferation of hBMSCs on mSCS-A-0, mSCS-A-0.05 and mSCS-A-0.1 cements, the Cell Counting Kit-8 (CCK-8, Dojindo) assay was used. Briefly, hBMSCs were cultured on cement at an initial density of 10^4 cells per sample for 1, 3 and 7 days. Then, 400 μL of the culture medium and 40 μL of the CCK-8 solution were added to each well at each time point and incubated at 37 °C for another 4 h. An aliquot of 100 μL was taken from each well and transferred to a fresh 96 well plate. The light absorbance of these samples was measured at 450 nm with a spectrophotometric microplate reader (Bio-Rad 680, USA). All the results were expressed as the optical density values minus the absorbance of blank wells.

Alkaline phosphatase (ALP) activity

To assess the development of the osteoblastic phenotype of hBMSCs grown on various types of cement, ALP activity was performed on days 7 and 14 after seeding 1×10^5 hBMSCs on each sample ($n = 3$) from the different groups. All the experiments were performed in triplicate in 24-well culture plates. At a predetermined time point, the culture medium was decanted and the cell layer was washed gently three times with PBS followed by washing once in cold 50 mM Tris buffer, and then the hBMSCs were lysed in 200 μL 0.2% triton X-100. Lysates were sonicated after centrifugation at 14 000 rpm for 15 min at 4 °C. 50 μL of the supernatant was mixed with 150 μL of the working solution according to the manufacturer's protocol (Beyotime). The conversion of *p*-nitrophenylphosphate into *p*-nitrophenol in the presence of ALP was determined by measuring the absorbance at 405 nm with a microplate reader (Bio-Rad 680, USA). The ALP activity was calculated from a standard curve after normalizing to the total protein content and the results are expressed in μM of *p*-nitrophenol produced per minute per milligram of protein.

Results and discussions

Microstructure characterizations of mSCS nanoparticles

The mSCS nanoparticles were prepared by simply substituting Ca with Sr during the mCS one-pot synthesis. Fig. 1A shows a TEM observation image of the mSCS nanoparticles. The picture clearly demonstrates the spherical morphology of the mSCS, though these nanospheres were agglomerated to some extent. The size of all the nanoparticles was narrowly distributed in the range of 200–300 nm, which coincides with the dimensions of mCS products reported formerly.[34] The inset zoomed-in picture clearly shows nanopores of the mSCS without order. The elemental mapping and EDX spectrum in Fig. 1 indicate the elemental compositions of mSCS materials. From Fig. 1B it is concluded that Ca^{2+} and Sr^{2+} homogeneously dispersed in the Si–O network, and the doping amount of Ca^{2+} was apparently higher than that of Sr^{2+}, which is confirmed by the element spectrum in Fig. 1D. N_2 sorption isotherms (Fig. 1C) present a hybrid pattern of type II and type IV isotherms. The mSCS nanoparticles exhibit a main capillary condensation jump between 0.4 and 0.6 of P/P_0, which is representative of penetrating cylindrical mesopores in accordance with the relatively narrow pore size distributions centered at around 3.1 nm (inset Fig. 1C). Another mild jump between $P/P_0 = 0.8$ and 1.0 may result from nanosphere stacking. The BET surface area was calculated to be 312 m^2 g^{-1}.

Pure mesoporous silica nanoparticles (MSNs) are now attracting an extremely intensive interest in the biomedical research field, particularly applying as drug delivery systems.[37] MSNs have shown good stability, super high surface area, adjustable mesopore structure and modified surfaces, and therefore MSNs have superior properties to control the drug load and release. However, the silica has issues of degradation and also apatite deposition on material surfaces when implanted to regenerate bones.[38] One of the most effective solutions to increase the bioactivity of silica is a calcium dopant.[39] The addition of calcium into the Si–O–Si network damages the integrity of the mesopore walls and thus accelerates the degradation rate. Moreover, the release of calcium ions is likely to induce a fast silicon-rich layer formation, which then draws apatite precipitation.[16] Considerable literature reports the fabrication and properties of mesoporous calcium silicate

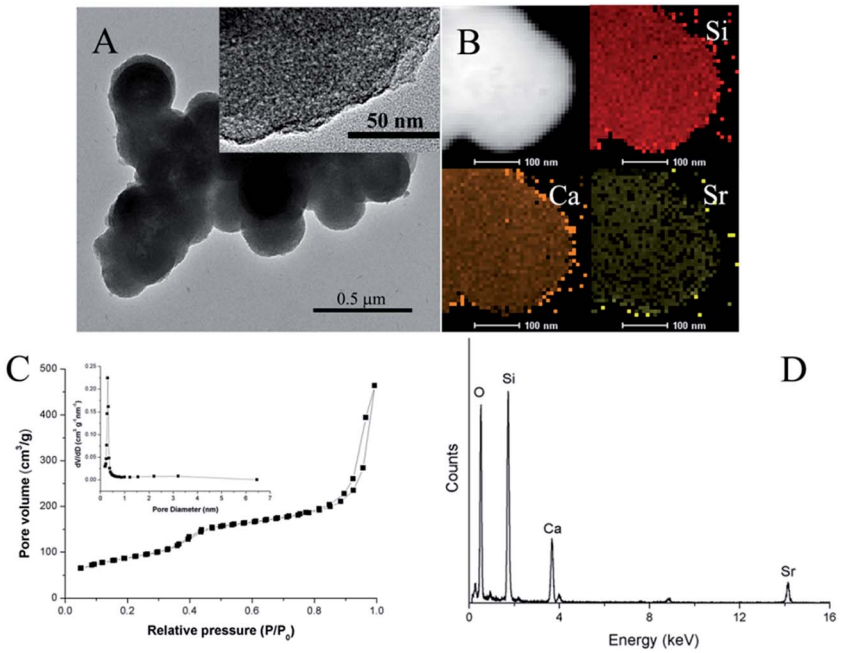

Fig. 1 (A) TEM image (inset: zoomed-in TEM image), (B) elemental mapping, (C) N_2 sorption isotherms and pore size distribution (inset) and (D) EDX spectrum of mSCS nanoparticles.

or SiO–CaO bioglass nanoparticles, and quite a few of them showed promising results in the repair of bone defects. In this study, we additionally substituted part of the calcium with strontium, which is also a crosslinker agent of an alginate hydrogel. Strontium addition did not remove the mesopores and the BET surface area of the mSCS nanoparticles remained as high as about 300 $m^2\ g^{-1}$. The size of the mesopores was large enough to encapsulate most chemotherapeutic drugs, such as osteoporosis bisphosphonates, antibiotics, osteogenesis promoter vitamins and so on.

Injectability of mSCS-A composite cement

The injectability of pastes was represented by measuring the percentage of residue materials after being pushed out. In the first 10 seconds, GDL incorporation did not produce a significantly increased injectability compared to that of mSCS-A-0. However, 2 minutes later, apparently more mSCS-A-0.05 and mSCS-A-0.1 samples can be injected out. For example, less than 5% of mSCS-A-0.1 pastes were left in the syringe, which indicated that mSCS-A-0.1 composites formed a coherent whole and then were readily extruded continuously. The result demonstrated that GDL hydrolysis took time to trigger the Ca^{2+}/Sr^{2+} ion release. Thereafter, ion-linked alginate gels knitted mSCS nanoparticles together and united the two constituents as one. On the other hand, Fig. 2 shows that a similar amount of mSCS-A-0.05 cement was extruded to mSCS-A-0.1 samples.

It is widely accepted that the applicability of injectable and *in situ* forming biomaterials largely depends on self-setting characteristics.[40] Here in this study, the injectability of mSCS–alginate composites was more reliant on the form of alginate. Viscous sodium alginate solutions mixed with mSCS particles resulted in a thick paste, which was difficult to inject through normal syringes and nozzles, and the sticky situation might be more serious as time passes after the loss of water. However, the formation of an alginate hydrogel decreases the viscosity by a large extent, and avoids mSCS–alginate composites sticking to the squeeze containers and are easy to inject. The whole gel-combined system is able to maintain unity and an integrated shape. In addition, the hydrogel could encapsulate all the inorganic nanoparticles together and then prevent the powder from leaking out. It is considered that free nanoparticles may exert potential bio-toxicity to the surrounding tissues, and thus the rapid gelation of alginate in mSCS-A-0.05 and mSCS-A-0.1 cements effectively preserves the mSCS materials.

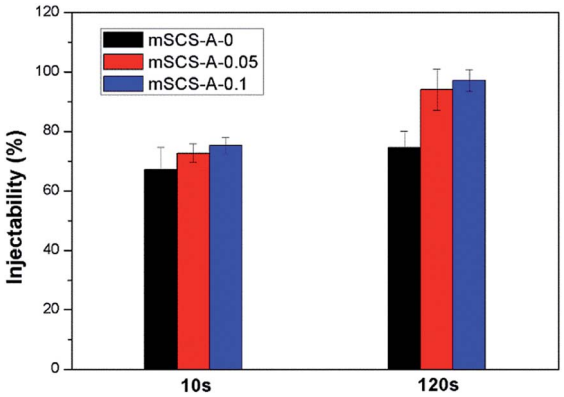

Fig. 2 Injectabilities of mSCS-A composite cements with different amounts of GDL, represented by the percentage of materials that remained in the syringes after the extrusion tests.

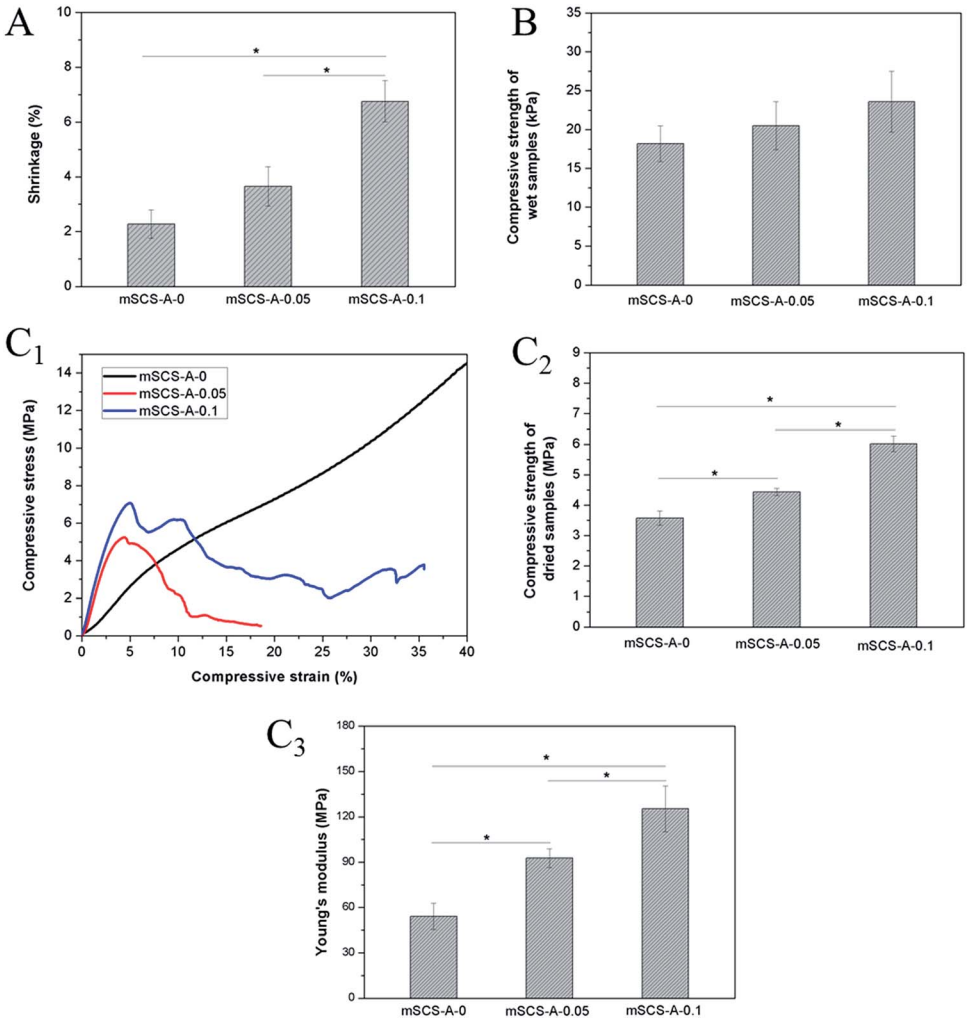

Fig. 3 (A) Shrinkage of the three types of mSCS–alginate cement after vacuum drying; (B) compressive strength of raw wet mSCS–alginate cement; (C_1) stress–strain curves, (C_2) compressive strength and (C_3) Young's modulus of mSCS-A-0, mSCS-A-0.05 and mSCS-A-0.1 cements.

Compressive strength

Fig. 3 summarizes the mechanical properties of both raw and dewatering mSCS-A composite cements. Fig. 3A illustrates the shrinkage degree while the water enriched cement was dried, and decreasing the GDL content apparently led to less shrinkage according to Fig. 3A. mSCS-A-0.1 cylindrical samples showed a mean $6.76 \pm 0.75\%$ contraction in diameter or height, whereas mSCS-A-0 samples without GDL had a much smaller contraction of about 2%. The reason might be attributed to the alginate gel tightening up the powder materials compared to alginate solution; when the water in the hydrogel is lost, the large pores created by the water would collapse to some extent. Nevertheless, the compressive strength of the wet mSCS-A-0.1 cement was relatively higher than that of the GDL-free cement, as shown in Fig. 3B. The more integrated structures of mSCS-A-0.05 and mSCS-A-0.1 led to higher pressure loadings, while alginate served only as an adhesive of the mSCS particles in the mSCS-A-0 samples and resulted in a loosely-structured mSCS-A-0 cement.

The mechanical strength data of the dried samples are shown in Fig. 3C. Fig. $3C_1$ displays entirely different stress–strain curve patterns of the mSCS-A-0 dried samples compared with the mSCS-A-0.05 and mSCS-A-0.1 samples in which GDL was added. A clear yield point followed by rupture can be seen on the curves of the crosslinked cement. There is no observed rupture for the mSCS-A-0 cement, and the approximate linear stress–strain relationship ended at a 7% deformation, as the curve shows, and hence the compressive stress of 3.5 MPa at this point was recorded as its strength. The fact was that the mSCS-A-0 cylindrical samples were gradually pressed down and the mSCS-alginate mixtures were compacted during the compressive tests. The properties shown by the curve indicates a similarity of mSCS-A-0 to inorganic-reinforced polymer materials. The calculated strength and Young's modulus are plotted in Fig. $3C_2$ and C_3. Both mSCS-A-0.05 and mSCS-A-0.1 cements exhibit significantly higher strengths compared to the GDL-free ones.

The SEM images in Fig. 4 at different magnifications can explain the results above. First of all, from the top view the

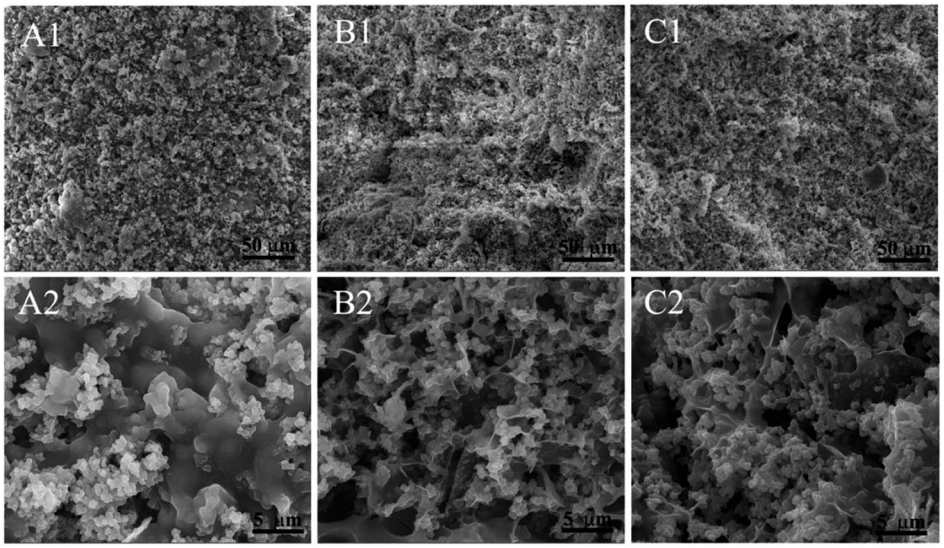

Fig. 4 SEM images of (A1 and A2) mSCS-A-0, (B1 and B2) mSCS-A-0.05 and (C1 and C2) mSCS-A-0.1 composite cements with different GDL contents.

mSCS nanospheres are clearly observed in all the composite cements, suggesting no morphology change throughout the whole cement formation. However, their connections between the mSCS nanoparticles and alginate macromolecules were rather varied.

After water removal, without GDL addition and alginate gelation for sample mSCS-A-0, phase separations presented as mSCS particle agglomeration and pure alginate segregation. In contrast, the images showed that mSCS nanoparticles distributed much more homogeneously over the gel network for the mSCS-A-0.05 and mSCS-A-0.1 cements. Furthermore, mSCS particles encapsulated in a hydrogel strut could give out cations under slow hydrolysis of the GDL and form homogeneous cement. GDL hydrolysis produces gluconic acid, which etches the Si–O–Si walls and Ca/Sr species then break away. Ca/Sr cations crosslinked the alginate molecules and, therefore, tridimensional alginate hydrogel structures were successfully formed that prevented regional particle aggregation.

The mSCS-A-0.05 and mSCS-A-0.1 cements also showed less compacted and porous structures that were created from hydrogel drying. Although there was pore shrinkage and collapse during the vacuum desiccation, plenty of pores, ranged at around tens of micrometers, can be still observed. This demonstrates that alginate molecules crosslinked to each other and formed water-rich pores. These pores are supposed to provide cells with space to grow in, which is obviously beneficial for bone repair compared to the conventional dense injectable cement.[41] Conventional calcium salt cement (including calcium phosphate, calcium sulfate and calcium silicate, *etc.*) are produced on the basis of powder hardening *via* hydration reactions; hence, the initial pores among the ceramic particles are filled by the hydrate products. Therefore, these densified cements can play a main role in filling the bone defects and supply an osteoconductive substrate as they also possess relatively high strengths. On the other hand, although having sufficient giant pores, injectable pure macromolecule hydrogels are too fragile to load any body weight. The irresistibility to forces of impact, shear and stress may lead to a falling apart of the pure alginate hydrogels. Therefore, on the premise of being implanted in non-loading areas, the composites of mSCS–alginate are likely to provide a rather strong support over a period of time after the injection, and at the same time offer cells some growth spaces.

Apatite deposition ability

The apatite-deposition was studied by SEM and an energy dispersive spectrometer after 3 days of SBF immersion. The results are shown in Fig. 5. It can be noticed that the surfaces of both mSCS particles and alginate polymers were roughened by lots of small bumps and clusters. One representative area of mSCS-A-0.05 was magnified to obtain more detail. The zoomed-in picture of the selected area (black frame) in Fig. 5B1 confirmed new apatite mineralization on the surfaces. Additional EDS spectra (Fig. 5A2–C2) of the surfaces after mineralization detected obvious characteristic peaks of Ca and P elements for all three groups of cement. The Ca/P molar ratios of deposition on mSCS-A-0, mSCS-A-0.05 and mSCS-A-0.1 cements were quasi-quantitatively calculated to be 1.34, 1.22 and 1.09, respectively, which were lower than the 1.67 of hydroxyapatite and indicate the formation of calcium-deficient carbonated apatite with a lower crystallinity degree. Another reason for the low Ca/P ratio could be that strontium phosphate precipitated as well to form an external layer on the scaffold surface instead of a calcium one.

In the physiological environment, the ability to induce a bone-like mineral on the surface of biomaterials is an essential property to determine the bonding with living bone. Mesoporous calcium silicate materials have been reported to improve the apatite formation of pure polymers both *in vitro*

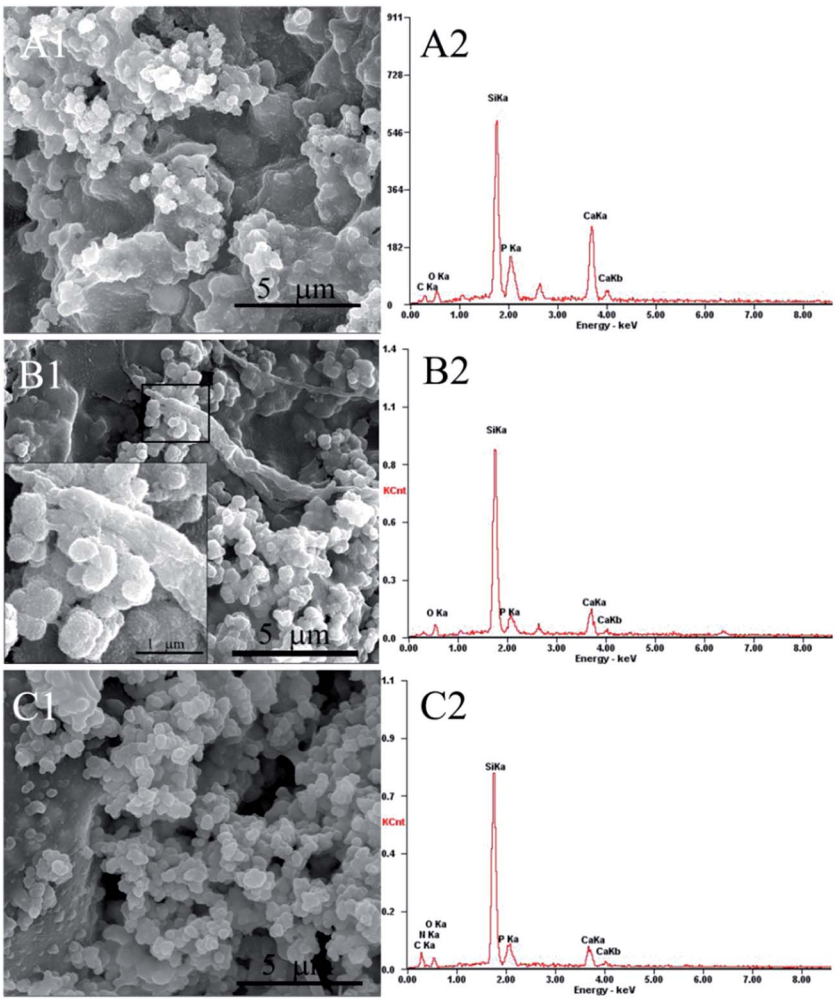

Fig. 5 SEM images and EDS analysis of mSCS-A composite cement surfaces after immersion in SBF for 3 days, (A1 and A2) mSCS-A-0, (B1 and B2) mSCS-A-0.05 and (C1 and C2) mSCS-A-0.1 cement.

and *in vivo*. The mesopore structure and super high surface area could accelerate the apatite deposition, including processes of Ca^{2+} release, ion exchange, silanol group enrichment and calcium salt deposition.[42] Therefore, it was worth evaluating whether mSCS still retained its apatite-inducing ability after the cations had released to crosslink alginate molecules. The EDS and SEM results demonstrated that the Ca^{2+}/Sr^{2+} ionic release triggered by GDL hydrolysis did not influence the bioactivity of the mSCS/alginate cement. The reasons are possibly contributed by two factors. Since the Ca^{2+}/Sr^{2+} ions were doped primarily in the Si–O–Si network and did not occupy the Si sites, they can quite easily leave the mSCS framework, and the

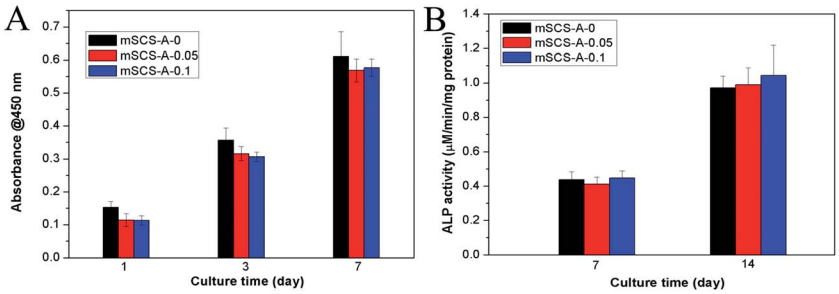

Fig. 6 (A) Proliferation of hBMSCs cultured on mSCS-A-0, mSCS-A-0.05 and mSCS-A-0.1 cements for 1, 3 and 7 days. (B) ALP activity of hBMSCs cultured on mSCS-A-0, mSCS-A-0.05 and mSCS-A-0.1 cements for 7 and 14 days, respectively.

crosslinking of alginate G blocks did not consume the Ca^{2+}/Sr^{2+} entirely. Besides, it is proved that the stability of calcium phosphate is higher than that of calcium alginate, and thus the calcium species anchored in the alginate hydrogels would precipitate with PO_4^{3-} ions from the SBF soaking.[43]

Cell culturing

In Fig. 6A, the CCK-8 assay revealed that cell proliferation gradually increased with a prolonged culturing time and all the specimens supported hBMSC cell adhesion and viability. It was noted that GDL incorporation caused an extremely subtle reduction in the O.D. value for the mSCS-A-0.05 and mSCS-A-0.1 cements referenced to the mSCS-A-0 cement, though the differences were not significant.

The intracellular ALP level was measured to observe the functional osteogenic activity of the cells, as shown in Fig. 6B. At both culture times (7 and 14 days), the ALP activity of the hBMSCs cultured on all three groups of cements showed similar values (Fig. 6B). This result suggested that the osteogenic differentiation of hBMSCs did not show any sharp distinction.

Conclusions

A novel approach is proposed in the present study to synthesize an *in situ* form of injectable cement composed of an alginate hydrogel and mesoporous Sr-containing calcium silicate nanoparticles. The formation of an alginate-mSCS composite cement is based on local Ca^{2+}/Sr^{2+} ion release from the mSCS *via* GDL hydrolysis, which then internally crosslink the alginate. The alginate hydrogel with mSCS nanoparticles encapsulated within has improved the injectability of the whole system. The compressive strength and integrity of the cement could be controlled by varying GDL contents. In contrast to dense cement or pure polymer hydrogels, the alginate–mSCS composite cements have the combined advantageous properties of high porosity, and a stronger and easy to handle strut. In addition, the cement can induce an apatite deposit on the implant material surface in only 3 days. The cements have been proved to be biocompatible and able to support hBMSC proliferation as well as osteogenesis differentiation.

Acknowledgements

The authors gratefully acknowledge the support of the National Natural Science Foundation of China (No. 81271998) and National High-Tech Research and Development Program (863-Project, No. 2015AA020316).

References

1 E. S. Place, N. D. Evans and M. M. Stevens, *Nat. Mater.*, 2009, **8**, 457–470.
2 T. Cordonnier, J. Sohier, P. Rosset and P. Layrolle, *Adv. Eng. Mater.*, 2011, **13**, B135–B150.
3 L. L. P. Hench and H. A. Paschall, *J. Biomed. Mater. Res.*, 1973, **7**, 25–42.
4 R. Langer and D. A. Tirrell, *Nature*, 2004, **428**, 487–492.
5 J. B. Dou, C. H. Sprague, L. Chen, Z. Q. Wang and S. F. Wang, *Materials Technology*, 2015, **30**, B273–B282.
6 H. C. Kroese-Deutman, P. Q. Ruhe, P. H. M. Spauwen and J. A. Jansen, *Biomaterials*, 2005, **26**, 1131–1138.
7 S. K. Mallapragada and B. Narasimhan, *Biomaterials*, 2002, **23**, 4305.
8 M. Bohner, *J. Mater. Chem.*, 2007, **17**, 3980–3986.
9 B. Balakrishnan and A. Jayakrishnan, *Biomaterials*, 2005, **26**, 3941–3951.
10 Y. S. Pek, M. Kurisawa, S. Gao, J. E. Chung and J. Y. Ying, *Biomaterials*, 2009, **30**, 822–828.
11 T. E. L. Douglas, W. Piwowarczyk, E. Pamula, J. Liskova, D. Schaubroeck, S. C. G. Leeuwenburgh, G. Brackman, L. Balcaen, R. Detsch, H. Declercq, K. Cholewa-Kowalska, A. Dokupil, V. M. J. I. Cuijpers, F. Vanhaecke, R. Cornelissen, T. Coenye, A. R. Boccaccini and P. Dubruel, *Biomed. Mater.*, 2014, **9**(045014), 1–14.
12 A. Memic, H. A. Alhadrami, M. A. Hussain, M. Aldhahri, F. Al Nowaiser, F. Al-Hazmi, R. Oklu and A. Khademhosseini, *Biomed. Mater.*, 2016, **11**(014104), 1–16.
13 W. C. Xue, A. Bandyopadhyay and S. Bose, *Acta Biomater.*, 2009, **5**, 1686–1696.
14 X. Li, J. L. Shi, Y. F. Zhu, W. H. Shen, H. Li, J. Liang and J. H. Gao, *J. Biomed. Mater. Res., Part B*, 2007, **83**, 431–439.
15 W. Xia and J. Chang, *Microporous Mesoporous Mater.*, 2008, **108**, 345–351.
16 G. F. Hu, R. F. Quan, Y. M. Chen, D. W. Bi, X. S. Jiang, X. F. Li and J. Y. Li, *RSC Adv.*, 2016, **6**, 57131–57137.
17 M. Zhu, J. H. Zhang, S. C. Zhao and Y. F. Zhu, *J. Mater. Sci.*, 2016, **51**, 836–844.
18 Y. F. Zhu, M. Zhu, X. He, J. H. Zhang and C. L. Tao, *Acta Biomater.*, 2013, **9**, 6723–6731.
19 H. Zreiqat, Y. Ramaswamy, C. T. Wu, A. Paschalidis, Z. F. Lu, B. James, O. Birke, M. McDonald, D. Little and C. R. Dunstan, *Biomaterials*, 2010, **31**, 3175–3184.
20 S. L. Peng, G. Q. Zhou, K. D. K. Luk, K. M. C. Cheung, Z. Y. Li, W. M. Lam, Z. J. Zhou and W. W. Lu, *Cell. Physiol. Biochem.*, 2009, **23**, 165–174.
21 P. J. Marie, D. Felsenberg and M. L. Brandi, *Osteoporosis Int.*, 2011, **22**, 1659–1667.
22 K. L. Lin, L. G. Xia, H. Y. Li, X. Q. Jiang, H. B. Pan, Y. J. Xu, W. W. Lu, Z. Y. Zhang and J. Chang, *Biomaterials*, 2013, **34**, 10028–10042.
23 E. Gentleman, Y. C. Fredholm, G. Jell, N. Lotfibakhshaiesh, M. D. O'Donnell, R. G. Hill and M. M. Stevens, *Biomaterials*, 2010, **31**, 3949–3956.
24 G. Orive, S. Ponce, R. M. Hernández, A. R. Gascón, M. Igartua and J. L. Pedraz, *Biomaterials*, 2002, **23**, 3825–3831.
25 M. Borgogna, G. Skjåk-Bræk, S. Paoletti and I. Donati, *J. Phys. Chem. B*, 2013, **117**, 7277–7282.
26 Y. A. Mørch, I. Donati, B. L. Strand and G. Skjåk-Bræk, *Biomacromolecules*, 2006, **7**, 1471–1480.
27 K. L. Chen, S. E. Mylon and M. Elimelech, *Langmuir*, 2007, **23**, 5920–5928.
28 E. S. Place, L. Rojo, E. Gentleman, J. P. Sardinha and M. M. Stevens, *Tissue Eng., Part A*, 2011, **17**, 2713–2722.

29 H. Y. Song, W. T. Yu, M. Gao, X. D. Liu and X. J. Ma, *Carbohydr. Polym.*, 2013, **96**, 181–189.
30 Y. Y. Zhao, M. T. Carvajal, Y. Y. Won and M. T. Harris, *Langmuir*, 2007, **23**, 12489–12496.
31 G. Turco, E. Marsich, F. Bellomo, S. Semeraro, I. Donati, F. Brun, M. Grandolfo, A. Accardo and S. Paoletti, *Biomacromolecules*, 2009, **10**, 1575–1583.
32 B. B. Crow and K. D. Nelson, *Biopolymers*, 2006, **81**, 419–427.
33 Y. Han, Q. Y. Zeng, H. Y. Li and J. Chang, *Acta Biomater.*, 2013, **9**, 9107–9117.
34 C. T. Wu, J. Chang and W. Fan, *J. Mater. Chem.*, 2012, **22**, 16801–16809.
35 T. Kokubo and H. Takadama, *Biomaterials*, 2006, **27**, 2907–2915.
36 T. Matsubara, K. Suardita, M. Ishii, M. Sugiyama, A. Igarashi, R. Oda, M. Nishimura, M. Saito, K. Nakagawa, K. Yamanaka, K. Miyazaki, M. Shimizu, U. K. Bhawal, K. Tsuji, K. Nakamura and Y. Kato, *J. Bone Miner. Res.*, 2005, **20**, 399–409.
37 Y. Chen, H. R. Chen and J. L. Shi, *Adv. Mater.*, 2013, **25**, 3144–3176.
38 Q. J. He, J. L. Shi, M. Zhu, Y. Chen and F. Chen, *Microporous Mesoporous Mater.*, 2010, **131**, 314–320.
39 A. Lopez-Noriega, D. Arcos, I. Izquierdo-Barba, Y. Sakamoto, O. Terasaki and M. Vallet-Regi, *Chem. Mater.*, 2006, **18**, 3137–3144.
40 A. M. Avachat and S. S. Kapure, *Int. J. Pharm.*, 2014, **477**, 64–72.
41 G. S. Lee, J. H. Park, U. S. Shin and H. W. Kim, *Acta Biomater.*, 2011, **7**, 3178–3186.
42 G. F. Wei, X. X. Yan, J. Yi, L. Z. Zhao, L. Zhou, Y. H. Wang and C. Z. Yu, *Microporous Mesoporous Mater.*, 2011, **143**, 157–165.
43 T. Braschler, A. Valero, L. Colella, K. Pataky, J. Brugger and P. Renaud, *Anal. Chem.*, 2011, **83**, 2234–2242.